Journal of Applied Fluid Mechanics, Vol. 17, No. 12, pp. 2545-2562, 2024.
Available online at www.jafmonline.net, ISSN 1735-3572, EISSN 1735-3645.
https://doi.org/10.47176/jafm.17.12.2715

A Numerical Investigation on the Effects of Vaned Diffusers on the Aerodynamic Performance of a Low Pressure-Ratio Methane Centrifugal Compressor

M. Anbarsooz[1†], M. Amiri[2] and E. Benini[3]

[1] *Department of Mechanical Engineering, Faculty of Advanced Technologies, Quchan University of Technology, Quchan, Iran*
[2] *Research and Development Department, Parto Sanat Pazh (PSP) Company, Mashhad, Iran*
[3] *Dipartimento di Ingegneria Industriale, Università di Padova, Padova, Italy*

†Corresponding Author Email: Anbarsouz@qiet.ac.ir

ABSTRACT

Vaned diffusers are widely used in centrifugal compressors due to their higher pressure-recovery coefficients compared to vaneless diffusers. In this study, the effects of the diffuser vanes' wrap angle and number of vanes on the aerodynamic performance of an industrial Methane centrifugal compressor with a pressure-ratio of 1.288 are studied using high fidelity steady-RANS numerical simulations. Three wrap angles (WA = 19.3°, 22.3° and 25.3°) and three number of vanes ($N_{Diff.}$ = 16, 20 and 24) are examined, while all the other geometrical and operational parameters are kept constant. Results showed that decreasing the wrap angle can enhance the choke flow rate of the compressor, with slight reduction in pressure ratio at low flow rates. However, increasing the diffuser wrap angle, intensifies the flow separation over the diffuser vanes. On average, the best aerodynamic performance of the compressor occurred at WA=22.3°. Results also showed that reducing the number of diffuser vanes enlarges the operating range of the compressor, however, the pressure ratio will be lower at the flow rates less than the design point. Conversely, higher pressure ratios will be achieved at the flow rates greater than the design flow rate. The optimal aerodynamic efficiency of the diffuser, considering both the pressure ratio and the total-to-total efficiency, was achieved when the N_{Diff} value was set to 20.

Article History

Received March 10, 2024
Revised June 14, 2024
Accepted July 4, 2024
Available online October 2, 2024

Keywords:

Centrifugal compressor
Vaneless Diffuser
Vaned Diffuser
CFD
Wrap Angle

1. INTRODUCTION

Centrifugal compressors are one of the essential components in a multitude of industries, among them are the air separation units, oil refineries, natural gas processing plants, petrochemical process plants, refrigeration industry, power generation plants, etc (Vagnoli & Verstraete, 2015; Hu et al., 2018). In this sub-class of turbomachines, kinetic energy is imparted to the fluid by a rotating impeller and then a portion of this energy will be converted into the static pressure in the diffuser (Niveditha & Gopi, 2023). The interaction between the impeller and diffuser within a centrifugal compressor is critically significant, as it accounts for approximately two-thirds of the compressor's overall losses in the diffuser (Teipel & Wiedermann, 1991; Dawes, 1995). It is mainly due to the complex and highly distorted flow discharged from the impeller into the diffuser (Rhie, 1985; El-Askary & Nasr, 2009; Wang et al., 2022).

Diffusers are categorized primarily into two types: vaneless and vaned. Vaneless diffusers are commonly used when a wider operating range or low costs are intended. However, vaned diffusers have to be used when higher pressure rise and efficiency are of concern (Sun et al., 2018). Vaneless diffusers are composed of two radial walls that can be arranged in parallel, or set to converge or diverge. In order to deswirl the flow, vanes are added to the diffusers which allow using small diameter ratios for the diffuser. However, even the vaned diffuser is commonly preceded by a vaneless diffuser. This vaneless space decreases the unsteadiness of the flow and reduces the Mach number reaching the leading edge of the diffuser vanes. On the other hand, adding the vanes imposes a blockage to the flow and generates a throat area between the vanes. To mitigate these effects, low solidity diffusers (Cellai et al., 2003) and partial vane diffusers have been introduced (Zhu et al., 2016).

Yet, various experimental investigations are conducted to reveal the flow characteristics inside the

diffusers. One of the pioneering experimental studies on the performance of vaneless diffusers is published by Dean and Senoo (Dean & Senoo, 1960) in 1960. They developed a simplified model for the unsteady and axially asymmetric flow discharged from the impeller into the diffuser. From 1960s up to 1990s, most of the studies on compressor and diffuser design have been performed experimentally such as Eckardt (Johnston & Dean, 1966; Baghdadi & McDonald, 1975; Eckardt, 1975; Senoo & Ishida, 1975; Baghdadi, 1977; Senoo et al., 1977; Inoue & Cumpsty, 1984).

From the 1990s, the computational fluid dynamics (CFD) simulations started its growing application in the field of turbomachinery, including the centrifugal compressors (Hah & Krain, 1990; Dawes, 1992; Koumoutsos et al., 2000). Kirtley and Beach (1992) conducted simulations of the flow within NASA's low-speed centrifugal compressor using a mean passage Navier-Stokes solver, complemented by an algebraic turbulence model based on RNG theory (Kirtley, 1991). Shum et al. (2000) demonstrated that, through Reynolds-Averaged Navier-Stokes (RANS) simulations, it is possible to determine an ideal radial gap size between the impeller and diffuser vanes to achieve the highest pressure increase in the impeller. Benini and Tourlidakis (2001) proposed one of the first CFD-based optimization studies for vaned diffusers based on coupling CFD with the Genetic Algorithms. To demonstrate the effectiveness of the proposed methodology, they compared the performance of a series of optimized diffusers with a real vaned diffuser in terms of the pressure recovery and efficiency. Engeda (2001a, b, 2003) created and evaluated eight distinct vaned diffusers with low solidity, each installed after the same impeller and tested at three different speeds of rotation. In their comparative analysis, they included two vaneless diffusers and a standard vaned diffuser with a solidity ratio of 1.15. Their result showed that the flow range become wider as the solidity decreases. The type of diffuser did not significantly impact the impeller's performance or the mass flow rate at which the inducer experiences stall.

Ziegler et al. (2003a, b) experimentally investigated the time-averaged and unsteady interactions of impeller and diffuser inside a test rig where the flat-wedge angle of the diffuser and the radial gap between the leading edge of the diffuser vanes and the impeller exit could be adjusted independently. Later, Boncinelli et al. (2007) numerically examined two diffuser geometries of the test results of Ziegler et al. (2003a, b) with different radial gaps with the main aim of separating steady effects from unsteady ones. Their numerical study showed that the flow unsteadiness has marginal effects on the stage performance. Reddy et al. (Reddy et al., 2004; Siva Reddy et al., 2007) examined how the angle settings of the vanes in a low-solidity type diffuser influence the overall performance of a stage in an industrial centrifugal compressor. The results illustrated that the diffuser vane's setting angle has significant effects on the blade loading and the overall stage performance. Issac et al. (2004) They conducted experimental research to determine how the position and height of the diffuser vanes affect the efficiency of a low-speed centrifugal compressor. The optimal vane height was identified as being 0.3 times the width of the diffuser for the compressor model examined. Additionally, the installation of partial vanes in a staggered arrangement on the hub and shroud resulted in a significant improvement in compressor efficiency. Smirnov et al. (2007) performed steady and unsteady numerical simulations for the open CFD test case, "Radiver" (Ziegler et al., 2003a, b), focusing on the fluid flow inside the diffuser. Their numerical results at the best efficiency point of the compressor showed that no considerable improvement can be seen in the predictions of the transient simulations compared to those of the steady-state simulations. Anish and Sitaram (Anish & Sitaram, 2009; Anish et al., 2013) conducted a numerical analysis on four distinct diffuser types—namely, vaneless, vaned, low solidity vaned, and partial vaned diffusers—to evaluate their impact on the performance of a centrifugal compressor across three varying radial distances from the diffuser vanes' leading edge to the impeller's exit. The highest pressure-recovery coefficient of the diffuser occurred for the vaned diffuser at the design flow coefficient. The compressor's highest efficiency was achieved when the diameter ratio, defined as the ratio of the diffuser leading edge diameter to the impeller exit diameter, was 1.15 at a low flow coefficient, 1.10 at the design flow coefficient, and 1.05 at a high flow coefficient. Robinson et al. (2012) compared different numerical techniques for modeling the impeller-diffuser interactions in a centrifugal compressor stage. They analyzed traditional steady-state simulations employing a mixing plane interface, a complete annulus simulation paired with a transient rotor-stator interaction approach, and an unsteady simulation utilizing a time-transformation (TT) technique. Their investigations revealed that the steady approach is capable of producing optimal aerodynamic designs with considerably lower computational costs. However, for evaluating the unsteady mechanical effects, the TT method can present reasonable results with significantly lower computational resources with respect to the full annulus simulations. Ubben and Niehuis (2014, 2015) carried out comprehensive experimental studies to assess how the radial gap between the impeller's outlet and the leading edge of the diffuser influences the operational characteristics of a centrifugal compressor. Furthermore, the effects of the diffuser vane angle and rotor speed are also studied. Their results showed that the clearance have a stabilizing effect on the compressor flow range and significantly enhances the compressor surge margin. Casey and Rusch (2014) introduced a one-dimensional analysis along with thorough experimental studies to align a vaned diffuser with a centrifugal compressor. An equation was suggested to calculate the necessary area of the diffuser's throat in proportion to the impeller's throat area at different design speeds.

Tamaki (2017) performed experimental investigations on seven diffuser vaned diffusers mounted downstream of a single impeller. They analyzed the effects of the vane setting angle on the diffuser and stage aerodynamic performance. Galloway et al. (2018a) proposed a novel casing treatment for the vaned diffusers to enhance the stable operating range of a high pressure ratio turbocharger at low flow rates and high pressure

Table 1 A concise review on the studies performed on the aerodynamic performance of vaned diffusers in centrifugal compressors

Ref.	Type of study	Ref.	Type of study
(Baghdadi & McDonald, 1975)	Exp.	(Skoch, 2003, 2005)	Exp.
(Krain, 1981)	Exp.	(Boncinelli et al., 2007)	Num. (RANS & URANS)
(Inoue & Cumpsty, 1984)	Exp.	(Siva Reddy et al., 2007)	Exp.
(Clements & Artt, 1989)	Exp.	(Smirnov et al., 2007)	Num. (RANS)
(Hohlweg et al., 1993)	Exp.	(Anish & Sitaram, 2009)	Num. (RANS)
(Dawes, 1995)	Num. (URANS)	(Robinson et al., 2012)	Num. (RANS & URANS)
(Deniz et al., 1998)	Exp.	(Everitt & Spakovszky, 2012)	Num. (URANS)
(Filipenco et al., 2000)	Exp.	(Anish et al., 2013)	Num. (RANS & URANS)
(Koumoutsos et al., 2000)	Num.(RANS & URANS)	(Casey & Rusch, 2014)	Exp.
(Benini & Tourlidakis, 2001)	Num. (RANS)	(Ubben & Niehuis, 2014, 2015)	Exp.
(Engeda, 2001a, b, 2003)	Exp.	(Everitt et al., 2017)	Num. (URANS)
(Kim et al., 2002)	Exp.	(Tamaki, 2017)	Exp.
(Cellai et al., 2003)	Exp.	(Galloway et al., 2018a, b)	Exp. & Num. (RANS & URANS)
(Ziegler et al., 2003a, b)	Exp.	(Fujisawa et al., 2019)	Exp. & Num. (RANS)
(Reddy et al., 2004)	Exp.	(Han et al., 2023)	Num. (RANS)
(Siva Reddy et al., 2005)	Num. (RANS)	(Ashrafi & Vo, 2024)	Num. (URANS)
(Issac et al., 2003, 2004)	Exp.		

Exp. = Experimental, Num. = Numerical, N.A. = Not Applicable, URANS = Unsteady RANS.

ratios. They also succeeded to enhance the stability of the compressor using porous throat diffusers with two different configurations, with a common side cavity and with individual side cavities (Galloway et al., 2018b). Recently, Fujisawa et al. (2019) described the evolution process of the diffuser's stall phenomenon (Everitt & Spakovszky, 2012; Pullan et al., 2015) using numerical and experimental investigations. Their CFD simulations using Detached Eddy Simulation (DES) turbulence model revealed that as the diffuser stall shifts from the shroud towards the hub, a tornado-type vortex generates close to the hub of the diffuser's leading edge. Then, boundary layer separation inside the vaneless space generates a throat area blockage at the hub. This blockage in the diffuser passage expands upstream towards the impeller passage and causes a stage stall. Han et al. (2023) employed steady RANS numerical modeling to investigate the formation and evolution of leading edge vortices of pipe diffusers inside a high pressure-ratio centrifugal compressor (Kenny, 1969). The fluid mechanics of the tip pair vortices are deeply discussed for various pipe diffusers. Ashrafi and Vo (2024) considered two compressors equipped with fishtail diffusers to study the effects of applying two passive flow control methods on the compressor's surge flow rate. Their findings suggest that employing passive flow control at the radial bend of the impeller shroud can yield substantially better results compared to its application at the leading edge of the impeller.

As reviewed above and summarized in Table 1, there are numerous studies on the performance of vaned diffusers employed in a variety of centrifugal compressors. However, the effects of the vanes' wrap angle have not been studied before. This study uses high-fidelity RANS simulations to examine how the performance of an industrial Methane centrifugal compressor is influenced by the wrap angle and the number of vanes of the diffuser. The detailed flow field around the diffuser vanes is visualized via presenting the streamlines and Mach number distributions around the diffuser vanes. The aerodynamic effectiveness of the diffuser is determined by evaluating the compressor's pressure increase, the overall efficiency based on total-to-total quantities, the static pressure recovery, and the diffuser's total pressure loss coefficients.

2. OPERATIONAL AND GEOMETRICAL SPECIFICATIONS OF THE COMPRESSOR

This study examines a single-stage methane centrifugal compressor, initially developed by Siemens. The working fluid is a blend of gases that comprises of 67.57% Methane, 22.71% Hydrogen, 4.36% Nitrogen, 2.73% Water, 1.84% Carbon Mono-oxide and 0.79% Carbon dioxide. Table 2 presents the design operating conditions of the compressor and also the geometric dimensions the impeller and diffuser.

The meridional contour and blade-to-blade view of the impeller are plotted in Fig. 1*a* and *b*, respectively. The blade mean-line distributions in the meridional coordinate are illustrated in Fig. 2. This 14-bladed impeller has a tip diameter of 0.18 m and an axial length of 0.216 m. Its diffuser consists of a vaneless diffuser with a diameter of 0.71 m and a vaned diffuser with 20 vanes. The diameters at the trailing edges of the diffuser vanes measure 0.933 m. Fig. 3 shows the diffuser and its

Table 2 Compressor's operating conditions and principal dimensions of the examined diffuser and impeller

Inlet temperature	45.0 °C
Inlet pressure	2.50 bar (absolute)
Inlet volumetric flow rate	45,827 m^3/h
Inlet mass flow rate	60,089 kg/h
Discharge pressure	3.22 bar (absolute)
Discharge temperature	70.0 °C
Rotational speed	9,531 rpm
Shaft power	1.032 MW
Impeller number of blades	14
Axial length of the impeller	0.216 m
Diameter of the hub	0.142 m
Impeller's suction diameter	0.434 m
tip diameter of the impeller (R_2 in Fig. 2)	0.613 m
Diameter of the vaneless diffuser (R_3 in Fig. 2)	0.710 m
Trailing edge radius of the diffuser vanes (R_4 in Fig. 2)	0.931 m
Diffuser's outer diameter (R_5 in Fig. 2)	0.99 m
Diffuser blade inlet angle	27 deg
Diffuser blade exit angle	40.5 deg
Diffuser number of blades	20
Diffuser blade wrap angle	22.3deg

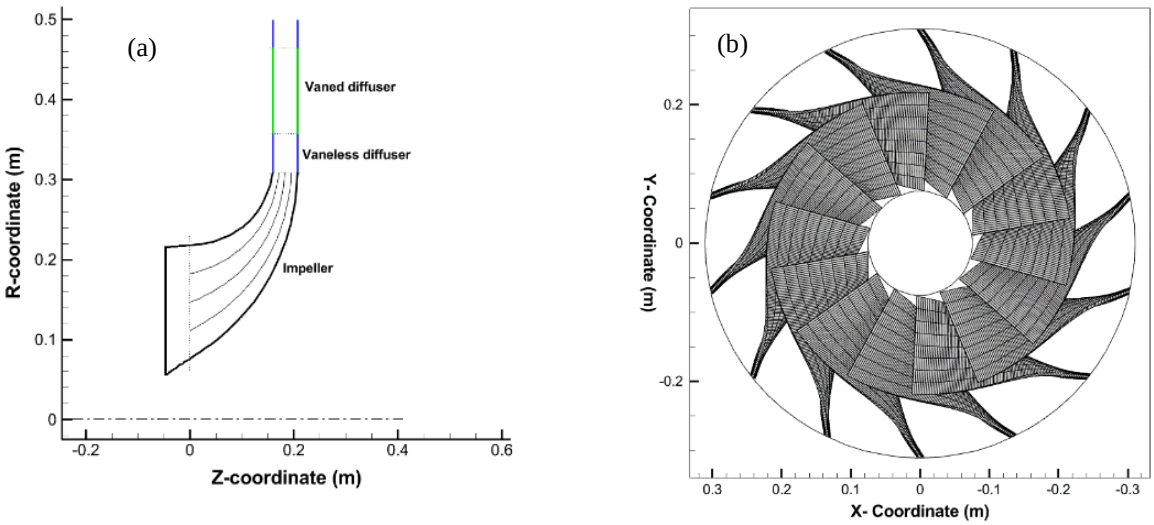

Fig. 1 (a) *Meridional* and (b) *blade*-to-blade view of the impeller

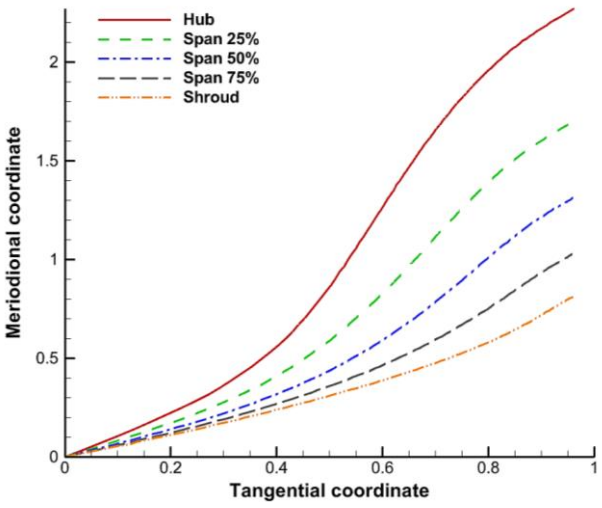

Fig. 2 Mean-line distributions of the impeller blade

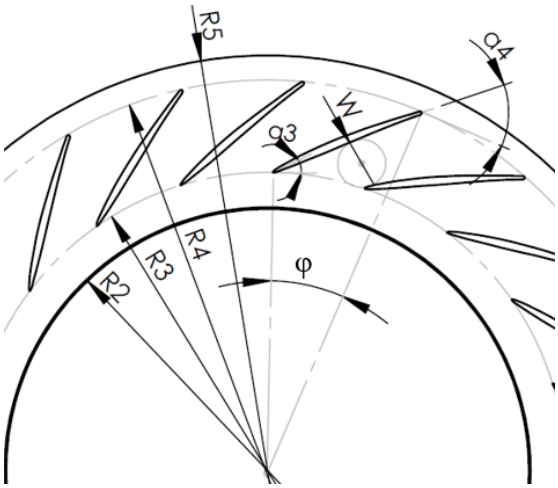

Fig. 3 Variables that illustrate the geometry of the vaneless region and the vaned diffusers

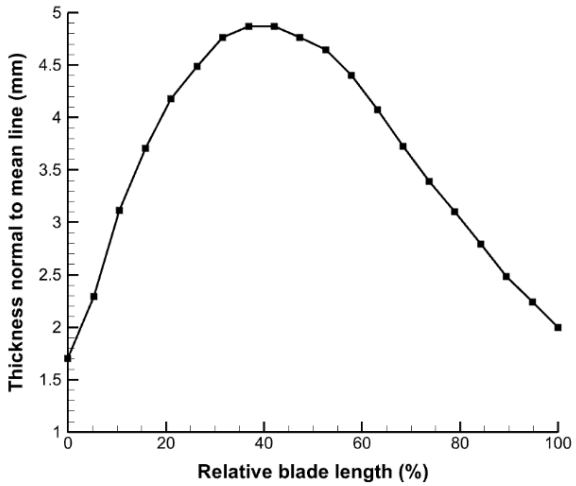

Fig. 4 Diffuser vane thickness distribution as a function of the relative blade length. In the spanwise direction, the vane thickness is uniform

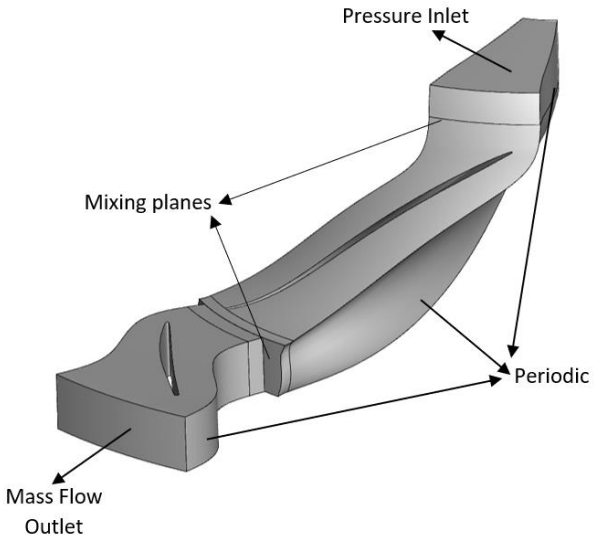

Fig. 5 Computational domain along with the implemented boundary conditions

main geometrical dimensions. The thickness distribution of the diffuser vanes, normal to the vane mean line, is presented in Fig. 4. The vane thickness is uniform in the spanwise direction.

3. NUMERICAL SETUP

3.1 Governing Equations, Computational Domain and Solver Settings

The steady RANS equations for the compressible turbulent flow with temperature-dependent thermophysical properties are considered as the governing equations. To complete the system of governing equations, three turbulence models are utilized: the Realizable *k-ε*, Shear-Stress-Transport (SST) *k-ω*, and Reynolds-Stress-Model (RSM). The appropriateness of these models for numerical simulation of this type of centrifugal compressors has been examined by several researchers (Robinson et al., 2012; Gibson et al., 2017; Halawa et al., 2015).

The resolution of the governing equations is achieved through the use of the Ansys-Fluent commercial software. (Anbarsooz, 2020; Anbarsooz et al., 2020, 2022), where the continuity and momentum equations are concurrently resolved through a coupled method. The upwind scheme with second-order accuracy is utilized to discretize the momentum, turbulence, density and pressure equations. To evaluate the cell gradients, the least-square cell-based method is employed. The accuracy of this method is comparable to that of the Green-Gauss node-based method and has shown superior accuracy (Holmes & Connell, 1989; Rausch et al., 1991).

The computational domain is composed of two stationary zones (the diffuser zone and the inlet zone) and one rotating zone (the impeller zone), as shown schematically in Fig. **5**. The impeller and diffuser zones are divided into 14 and 20 subzones, respectively, based on the number of impeller blades and diffuser vanes.

3.2 Boundary Conditions

Figure 5 illustrates the boundary conditions that have been established on different surfaces of the computational domain. A uniform and constant total pressure of P_0=0.25 MPa and total temperature of T_0=45C, is imposed at the inlet boundary. The stationary zones, which include the inlet and diffuser zones, are linked to the rotating impeller zone through the use of mixing planes (Jiao et al., 2009), where all the transport properties are conserved ensuring consistent flow across both frames of reference (Cornelius et al., 2014). The impeller blades, the hub and the shroud surfaces are considered as no-slip walls. A fixed mass flow rate is set at the diffuser zone's outlet surface. As the iterative solution reached the steady-steady condition, the computed total pressure at the diffuser's outlet is considered to calculate the pressure ratio (total-total) of the compressor. The employed methodology has been validated and used by several researchers (Jiao et al., 2009; Kianifar & Anbarsooz, 2011; Amiri & Anbarsooz, 2019; Anbarsooz, 2016).

The aerodynamic performance of the compressor has been evaluated in terms of the dimensionless quantities which are specific speed, N_s, work coefficient, ψ, and flow coefficient, φ. These dimensionless quantities are (Stewart, 2019):

$$\varphi = Q/ND^3 \tag{1}$$

$$\psi = gH/N^2D^2 \tag{2}$$

$$N_s = \frac{NQ^{\frac{1}{2}}}{H^{\frac{3}{4}}} \tag{3}$$

where N (rad/s) is the rotational speed, Q (m^3/s) volumetric flow rate, H (m) adiabatic head, and D (m) is the impeller diameter. For the compressor investigated in the current study, the corresponding dimensionless quantities at the design point are: φ=0.00580, ψ=0.00145 and N_s = 56.93. The efficiency (total-total) of

Table 3 Cell count of the examined grid densities and the relative error of the calculated pressure-ratios compared to the experimental data

Grid	Total number of cells	Pressure ratio	Percentage of relative error measured against the experimental data
Fine	882,011	1.301	1.01%
Medium	565,984	1.309	1.64%
Coarse	303,173	1.325	2.87%

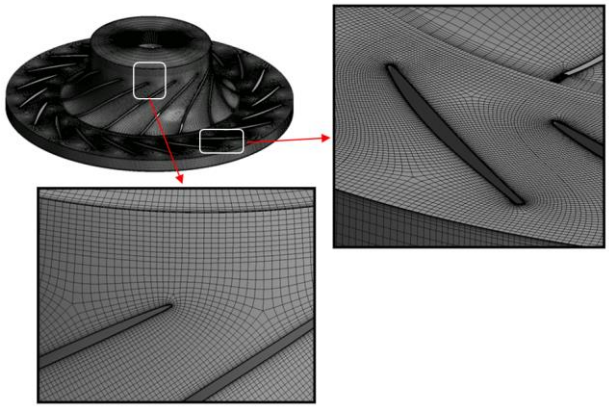

Fig. 6 Moderate density grid around the critical regions of the impeller and diffuser vanes

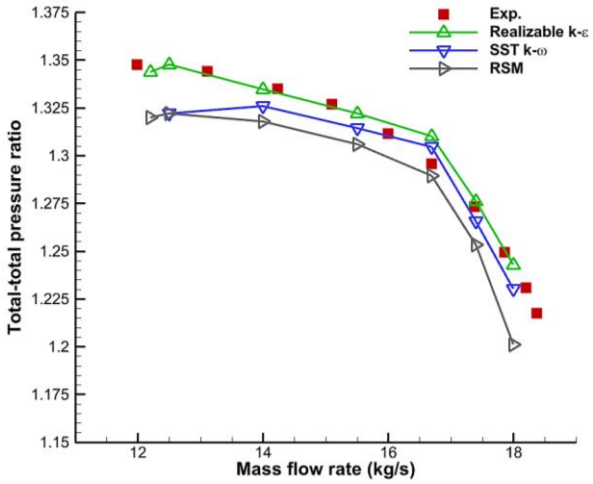

Fig. 7 Comparison of numerical outcomes derived from various turbulence models against the experimental data

the compressor based on the shaft's torque is defined as (Engeda, 2003):

$$\eta = \frac{\dot{m}(h_{02s} - h_{01})}{T\omega} \tag{4}$$

where ω is the angular velocity, T is the shaft torque, h_{02s} the isentropic total enthalpy at the diffuser outlet, and h_{01} is the total enthalpy evaluated at the inlet of the compressor.

3.3 Grid

The numerical domain is divided into elliptic cells of H-shape structure. To ensure the results are grid-independent, three grid resolutions, are generated. Table 3 presents the number of computational cells for three levels of grid resolution, designated as coarse, medium, and fine. Extra fine grids are applied at all walls of the domain, resulting in average y^+ values less than one. Furthermore, an enhanced wall treatment is utilized which is insensitive to the wall y^+ (Goldberg et al., 1998). Figure 6 shows the medium grid resolution, which is also magnified near the impeller and diffuser blades. The results of the grid-independency study are presented in Table 3, where the calculated values for the compressor's total-to-total pressure ratio are compared with those of the experiments at the design mass flow rates of 16.69 kg/s. According to Table 3, the results of the medium and fine grids are almost equal and therefore, the medium grid resolution is selected for the remainder of the simulations in this study.

4. Results and Discussions

4.1. Validation

In order to scrutinize the accuracy of the suggested numerical approach, the numerical results for the total-total pressure ratio at various flow rates are compared with those of the experiments in Fig. 7. The numerical outcomes are derived using three different turbulence models: the SST *k-ω*, Realizable *k-ε*, and RSM turbulence models. The experimental data are adopted from the compressor datasheet provided by the manufacturer. Results shows that all models have predicted the pressure ratio with an average relative error less than 5%. Among the tested turbulence models, the results of the Realizable *k-ε* turbulence model are in a better agreement with those of the experiments. As a result, the remainder of the simulations are carried out using this turbulence model.

The closer predictions of the Realizable *k-ε* turbulence model to experimental data might be due to several reasons; (*a*) This model is recognized for its exceptional efficacy in handling flows characterized by rotation, boundary layers with intense adverse pressure gradients, separation, and recirculation, (*b*) This model employs a refined approach for the transport equation of the dissipation rate, originating from the transport equation for the fluctuations of mean-square vorticity and (*c*) The realizable *k-ε* model incorporates constraints on realizability for turbulent Reynolds stresses, which results in enhanced accuracy in forecasting the dispersion of turbulence. These factors contribute to the realizable *k-ε* model's ability to more accurately simulate the turbulent flow characteristics of a centrifugal compressor, resulting in predictions that align more closely with experimental observations. However, the manufacturer did not provide the experimental data regarding the compressor's efficiency and therefore, the validation was not possible on the efficiency results. Instead, the validation has been

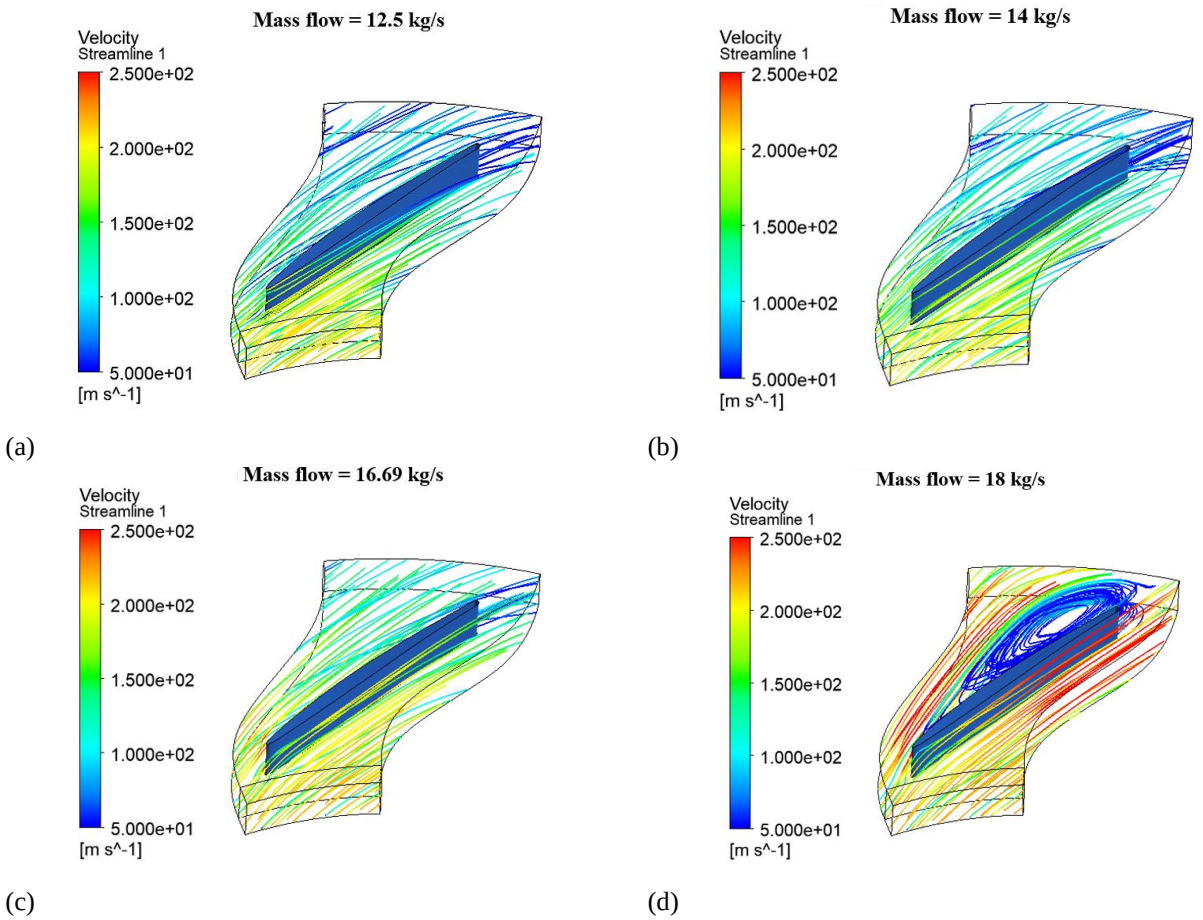

Fig. 8 Three dimensional streamlines around the diffuser vane at various mass flow rates for the $N_{Diff.}$=20

carried out for the Eckardt compressor in a previous paper (Benini, 2003) for both pressure-ratio and the total-to-total efficiency and they are not repeated here.

The three-dimensional streamlines around the diffuser blades at various mass flow rates (12, 14, 16.69 and 18 kg/s) for the $N_{Diff.}$ = 20 are presented in Fig. 8. The flow separation can be clearly seen at the flow rate of 18 kg/s due to larger incident angle. In order to quantify the incidence angle and also the effectiveness of the diffuser to change the flow direction, the mean flow angles at both the impeller and diffuser outlets are depicted in Fig. 9, corresponding to varying mass flow rates. As expected, as the flow rate increases, the average flow angle increases. It is because the meridional component of the velocity is larger at higher flow rates, while the blade tip velocity is constant.

On Fig. 9, the leading edge angle (vane inlet angle) and the trailing edge angle (vane outlet angle) of the diffusers' vanes are also depicted. The figure shows that the vane's angle at the leading edge is selected equal to the flow angle at the surge. In other words, the current diffuser works with positive incidence angle in its entire flow range. It prevents the occurrence of flow separation in the diffuser at low flow rates, however, strong flow separation appear at high flow rates, as can be seen in Fig. 8d.

The flow angle at the diffuser outlet is almost constant, with slight deviation close to the surge flow rate. The flow angle at the diffuser outlet is less than the trailing edge

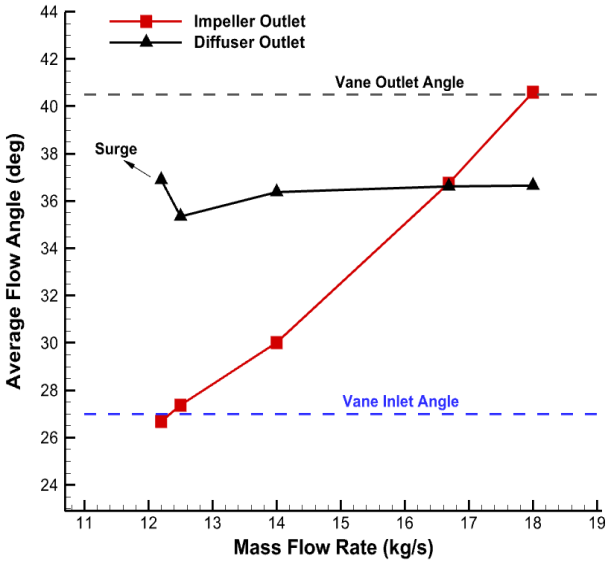

Fig. 9 Average flow angles at the outlets of both the impeller and diffuser, represented as a function of the flow rate

angle of the diffuser vane by about 4.5 degrees. The distributions of the flow angle at impeller outlet for different flow rates are presented in Fig. 10. It can be seen that the nonuniformity of the flow angle is more intense at lower flow rates.

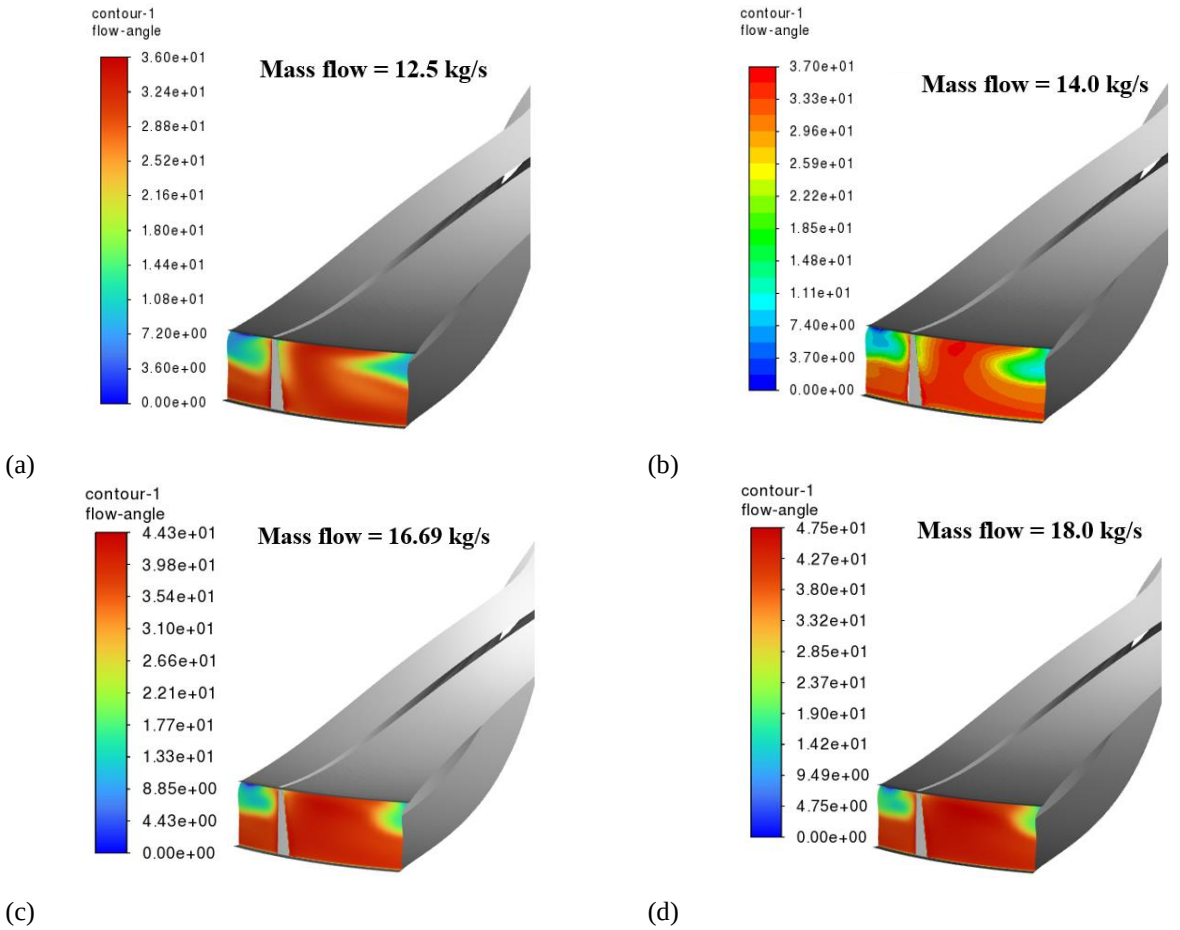

Fig. 10 Flow angle distributions at the impeller outlet at various flow rates. Angles are measured in degrees

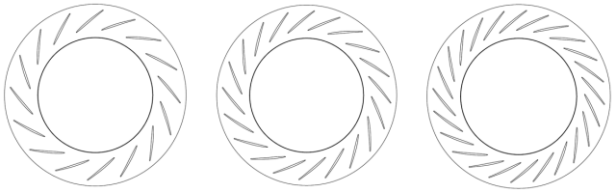

Fig. 11 Studied vaned diffuser with different number of vanes

4.2. Number of Diffuser Vanes

This part of the study explores the relationship between the diffuser's vane count and the compressor's performance. Three different number of vanes, $N_{Diff.}$ = 16, 20 and 24 are considered, while maintaining all other geometric and operational parameters unchanged as specified in Tables 2 to 4. Figure 11 shows the geometry of the diffusers with different number of vanes. The static pressure recovery coefficient, $C_{p,s}$, and the total pressure loss coefficient, $C_{p,t}$, are used to describe the diffuser performance. They are defined as follows (Li et al., 2018):

$$C_{p,s} = \frac{p_{static,outlet} - p_{static,inlet}}{p_{total,inlet} - p_{static,inlet}} \quad (5)$$

$$C_{p,t} = \frac{p_{total,inlet} - p_{total,outlet}}{p_{total,inlet} - p_{static,inlet}} \quad (6)$$

In fact, the static pressure recovery coefficient shows what portion of the inlet kinetic energy has been converted to the static pressure inside the diffuser and the total pressure coefficient shows the portion of the kinetic energy lost in the diffuser.

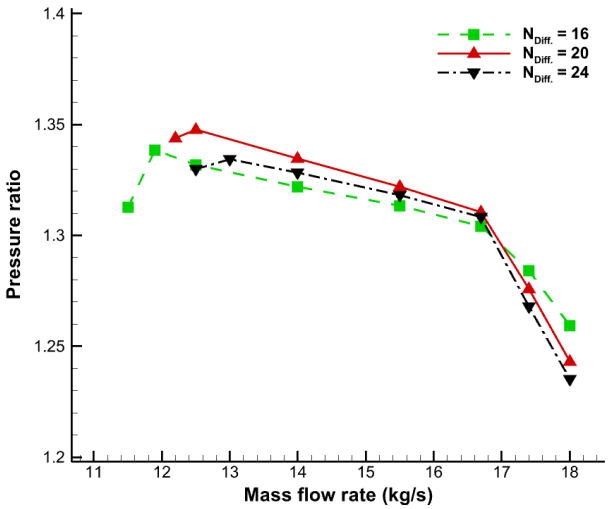

Fig. 12 Effects of the diffuser's number of vanes on the compressor pressure ratio (total-to-total)

The compressor's pressure ratio (total-to-total), depicted as a function of the mass flow rate, is illustrated in Fig. 12 for a range of diffuser vane counts. Increasing the number of diffuser vanes adds a local geometrical throat inside the diffuser zone and as a result, reduces the choked flow rate. According to Fig. 12, the choked flow

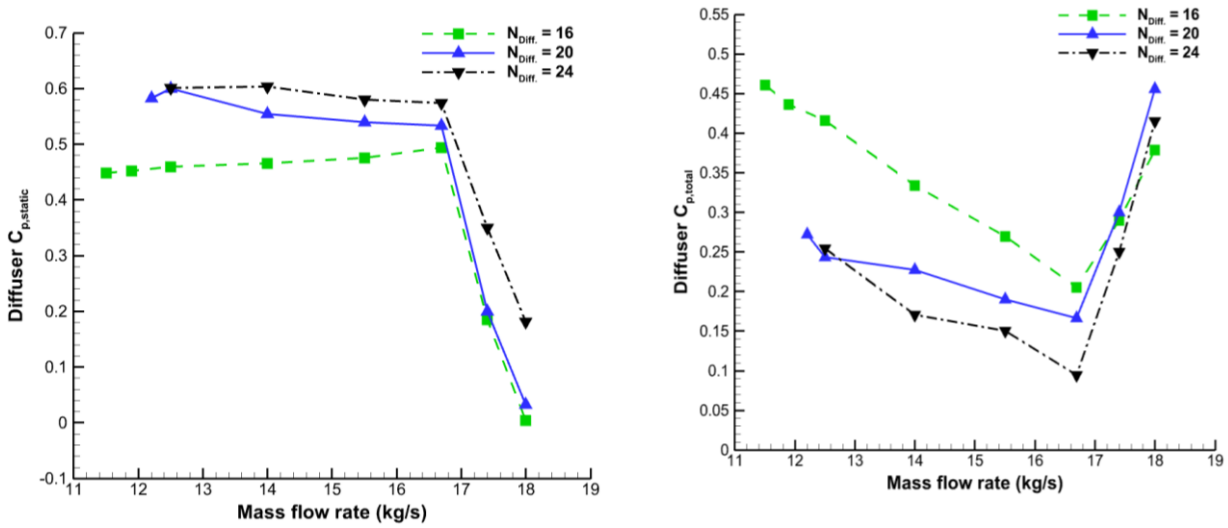

Fig. 13 Coefficients for (*a*) diffuser pressure recovery and (*b*) total pressure loss as functions of the flow rate, corresponding to different number of diffuser vanes

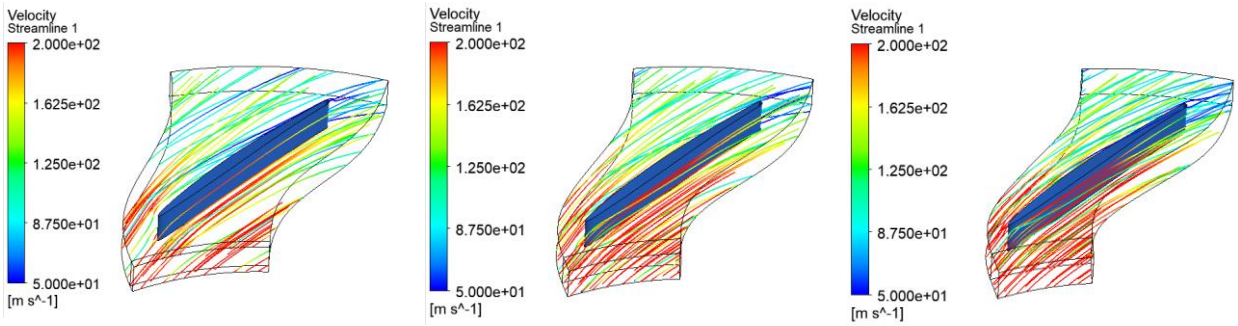

(*a*) $N_{Diff.}$ = 16 (*b*) $N_{Diff.}$ = 20 (*c*) $N_{Diff.}$ = 24

Fig. 14 Three-dimensional streamlines around the diffuser vanes at the flow of 16.69 kg/s, for various number of vanes

rate decreases as the number of diffuser vanes increases. At lower flow rates, however, the maximum pressure ratio has occurred for $N_{Diff.}$=20. This implies that there is an optimum number of vanes for the diffuser. Although increasing the number of vanes mitigates the flow slip at the diffuser outlet, the resultant frictional loss causes the pressure ratio to decrease. To quantitatively assess the aerodynamic efficiency of the diffuser, Fig. 13 plots both $C_{p,s}$ and $C_{p,t}$ in relation to the mass flow rate. According to Fig. 13*a*, the slope of the curves at the flow rates less than 16.69 kg/s for different number of diffuser vanes are modest, however, at larger mass flow rates, $C_{p,s}$ drops sharply as the flow rate increases. It is due to the large incidence angle of the diffuser vane at the design point (as can be observed in Fig. 9). Figure 13*b* shows that the minimum total pressure loss has also occurred at the flow rate of 16.69 kg/s, for all of the studied $N_{Diff.}$. To visualize the flow pattern around the diffuser vanes, the three-dimensional streamlines are depicted for various number of diffuser vanes at two mass flow rates of 14 and 16.69 in Fig. 14 and Fig. 15, respectively. As can be observed in these two figures, no separation region can be seen at the flow rate of 16.69 kg/s, however, at 18 kg/s large separation zones has been formed for various number of diffuser vanes.

The effects of the number of diffuser vanes on the Mach number distribution inside the diffuser zone are illustrated in Fig. 16 at different mass flow rates for various number of diffuser vanes. As expected, the Mach number increases by increasing the mass flow rate. Furthermore, increasing the number of diffuser vanes causes the Mach number to increase by creating smaller flow passage areas.

The total-total efficiency of the compressor versus flow rate is depicted in Fig. 17 for various number of diffuser vanes. The maximum efficiency for various $N_{Diff.}$ has occurred at the design flow rate of 16.69 kg/s. As mentioned before, at this flow rate the diffuser vane is operating at its maximum incidence angle before separation. The incidence angle at this flow rate is 9.5 degrees (as shown in Fig. 9). Fig. 17 also shows that the efficiency of the stage with $N_{Diff.}$ = 16 is higher at the flow rates greater than the design point, while $N_{Diff.}$ = 20 is better at the flow rates less than the design point. On average, $N_{Diff.}$ = 20 can be selected as the optimum number of vanes, among the examined cases in this study.

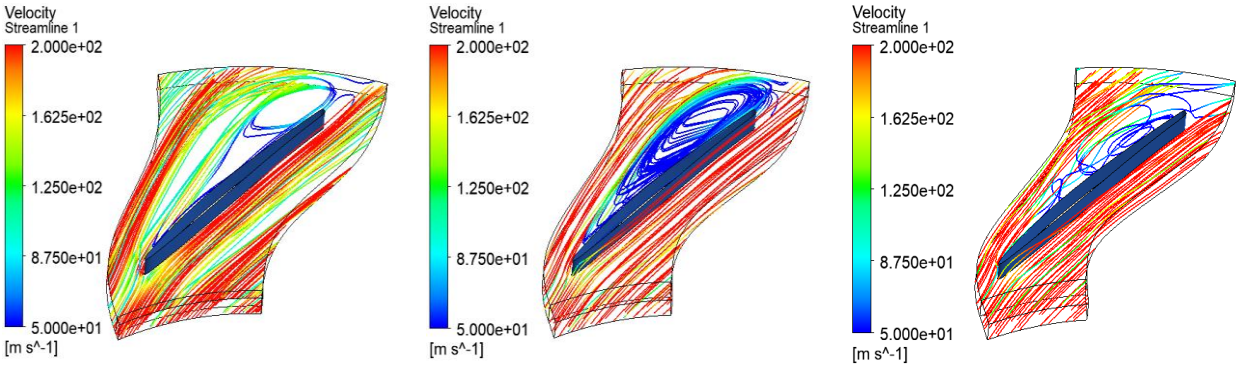

(*a*) $N_{Diff.}$ = 16 (*b*) $N_{Diff.}$ = 20 (*c*) $N_{Diff.}$ = 24

Fig. 15 Three-dimensional streamlines around the diffuser vanes at the flow of 18.0 kg/s, for various number of vanes

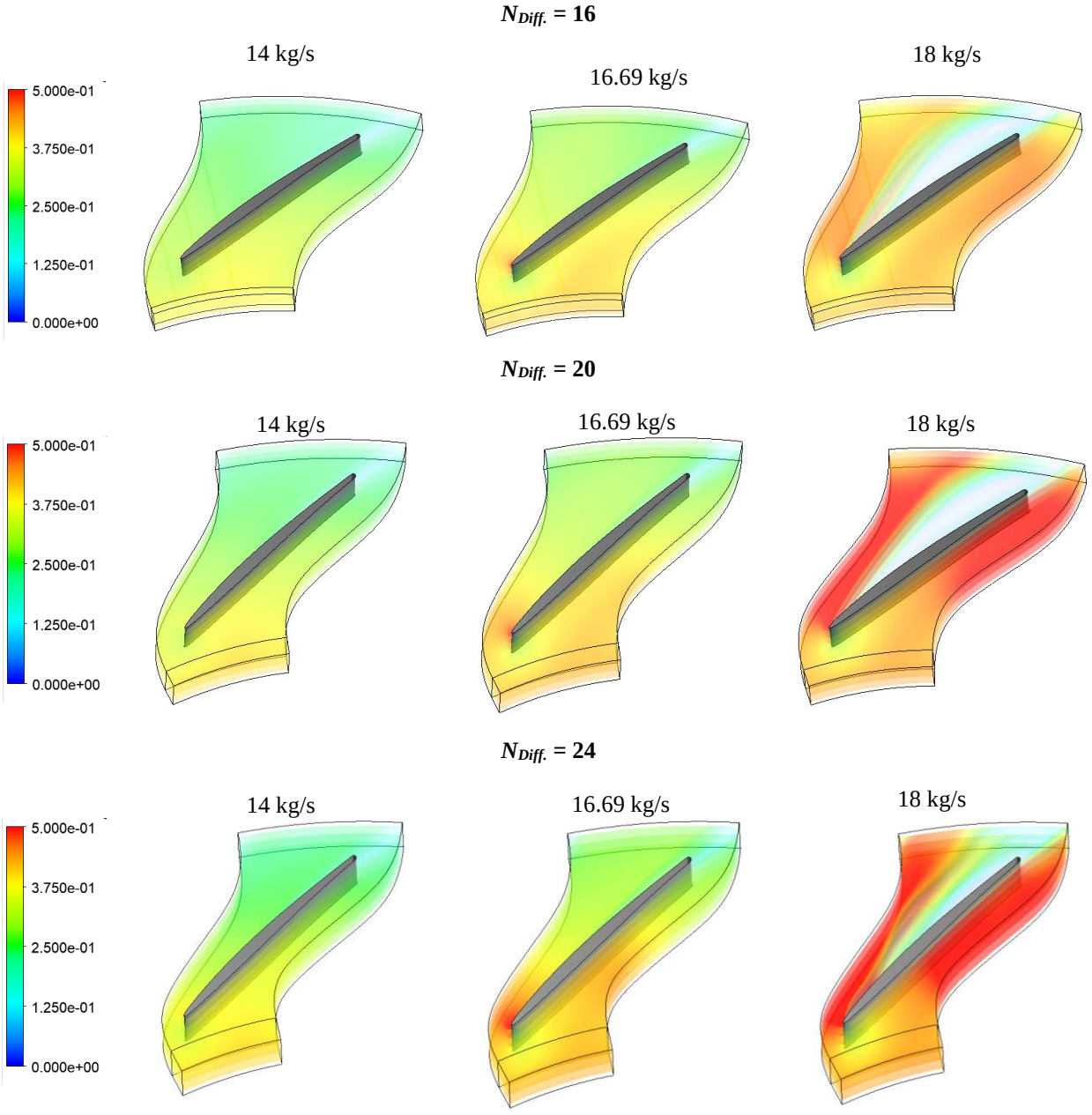

Fig. 16 Volume renderings of the Mach number distributions around the diffuser vanes at various mass flow rates and number of vanes

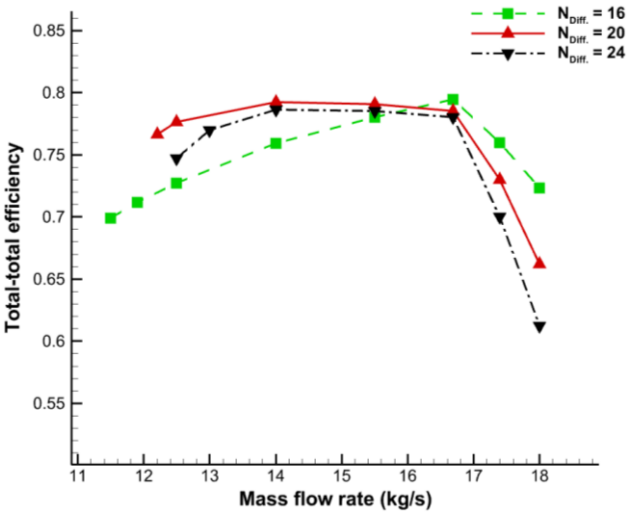

Fig. 17 Influence of the diffuser's vane count on the compressor's total-to-total efficiency

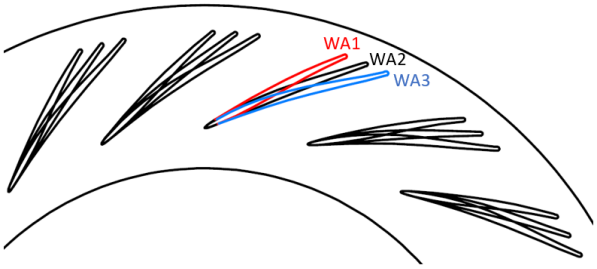

Fig. 18 Studied wrap angles (WAs) of the diffuser vanes. WA1 = 19.3º, WA2 = 22.3º and WA3 = 25.3º

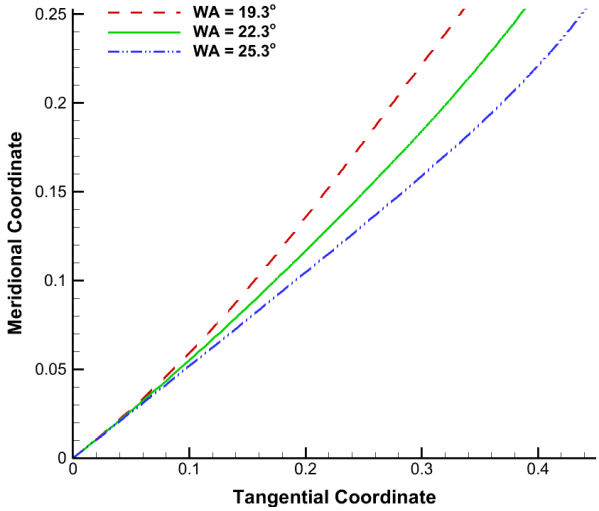

Fig. 19 Mean-line distributions of the studied diffuser vanes in the meridional-tangential coordinate system

4.3. Wrap Angle of the Diffuser Vanes

In this section, the effects of the diffuser vanes' wrap angle (WA) on the diffuser and compressor performance are analyzed. Three wrap angles are considered, which are: WA1 = 19.3º, WA2 = 22.3º and WA3 = 25.3º. The geometry of the examined diffuser vanes is plotted in Fig. 18. The mean-lines of the studied vanes in the meridional-tangential coordinate system are depicted in Fig. 19

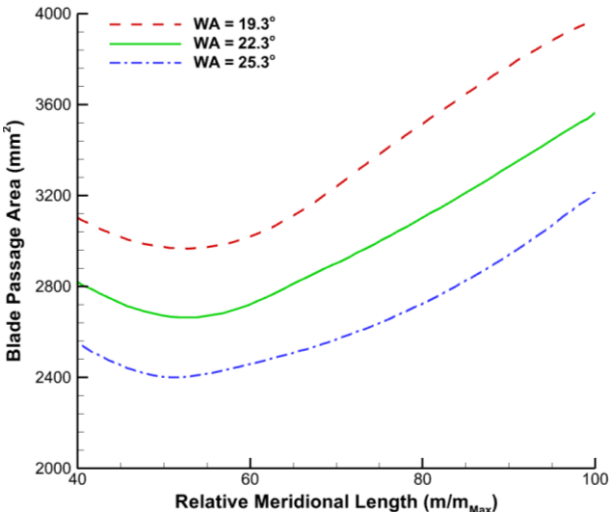

Fig. 20 Blade passage area as a function of the relative meridional length for various wrap angles

indicating that the curve length increases as the vane wrap angle grows. In other words, increasing the diffuser vane's wrap angle elongates the flow path inside the diffuser, resulting in higher friction losses and at the same time, lower pressure gradient inside the diffuser. However, as the wrap angle increases, the blade passage area decreases due to curvature effects as shown in Fig. 20.

Keeping all the other geometrical and operational properties constant, the numerical simulations are performed for the new diffuser vanes. The resultant pressure ratio and efficiency (total-to-total) of the compressor are plotted in Fig. 21.

As can be seen in Fig. 21*a*, for flow rates less than 16.69 kg/s, the pressure ratio and efficiency of WA = 22.3º is greater than the others. However, for the flow rates greater than 16.69 kg/s, the best performance has occurred at WA = 19.3º. Increasing the wrap angle has three effects: (*a*) the flow path increases and as a result the pressure gradient over the diffuser vane decreases, (*b*) the blade passage area decreases and the flow path increases, both leads to higher frictional losses (c) the flow has to rotate more in the tangential direction and as a result, the risk of separation over the vane surface increases.

The flow streamlines around the diffuser vanes with various wrap angles are plotted in Fig. 22 and Fig. 23 for the flow rates of 16.69 and 18.0 kg/s, respectively. It can be seen that at 16.69 kg/s, no considerable flow separation can be seen and only a small separation region has started to form at WA = 25.3º. At the flow rate of 18.0 kg/s, a large separation zone can be observed for both wrap angles of WA = 22.3º and WA = 25.3º. However, decreasing the wrap angle to 19.3º has eliminated the separation region and as a result, higher pressure ratio and efficiency has been obtained.

The corresponding Mach number distributions at various flow rates (14.0, 16.69 and 18.0 kg/s) and different wrap angles (WA = 19.3º, 22.3º and 25.3º) are presented in Fig. 24. This illustration distinctly demonstrates that the separation regions has narrowed the flow passage area and therefore, the Mach number has increases outside the separation region.

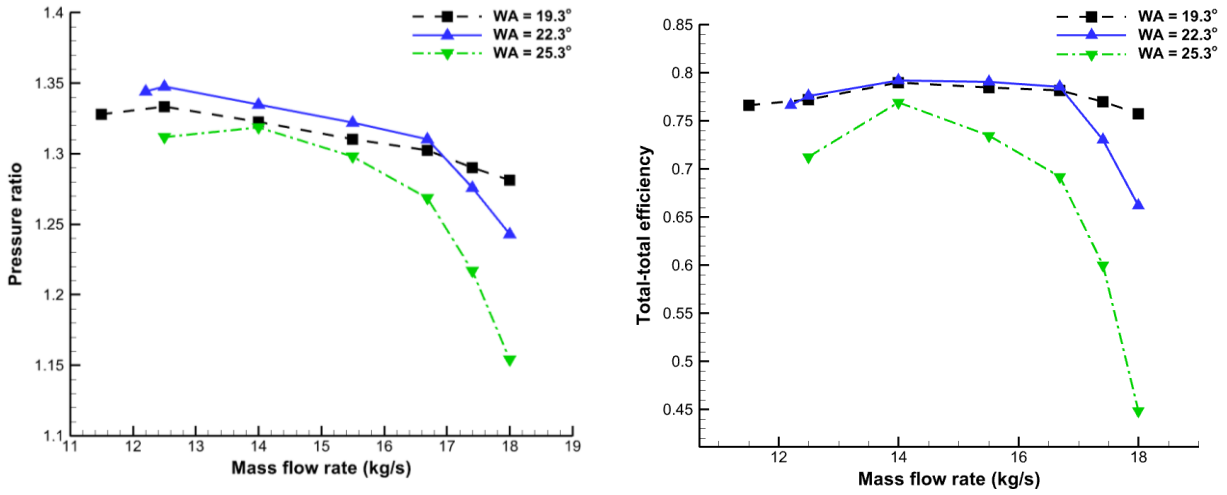

(*a*) (*b*)

Fig. 21 Effects of the diffuser vanes' wrap angle on (*a*) the pressure ratio and (*b*) efficiency

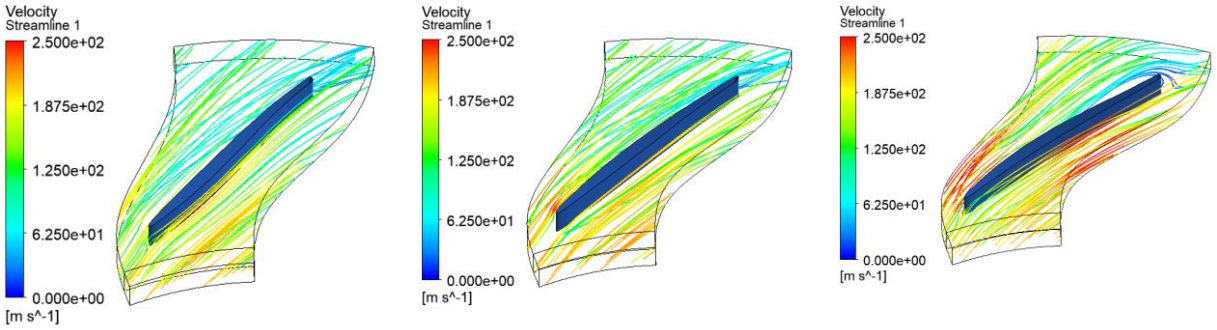

(*a*) WA1 = 19.3º (*b*) WA2 = 22.3º (*c*) WA3 = 25.3º

Fig. 22 Three-dimensional streamlines around the diffuser vanes at the flow rate of 16.69 kg/s, for various wrap angles

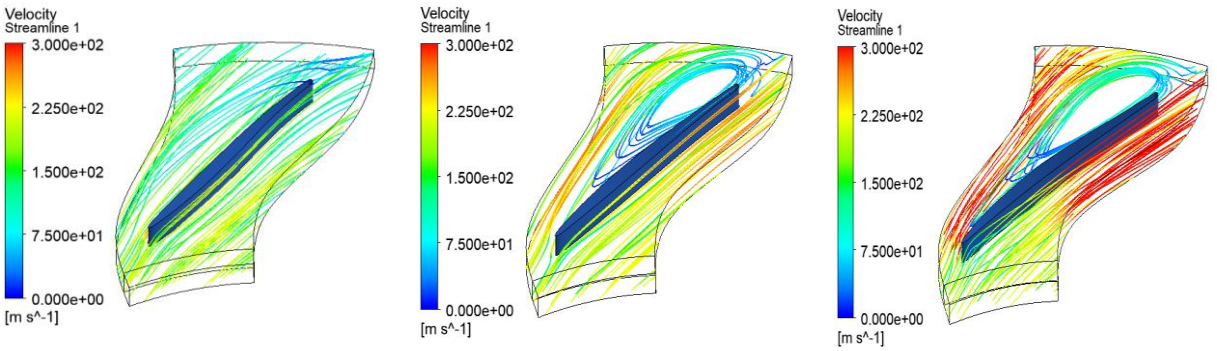

(*a*) WA1 = 19.3º (*b*) WA2 = 22.3º (*c*) WA3 = 25.3º

Fig. 23 Three-dimensional streamlines around the diffuser vanes for various wrap angles (flow rate = 18.0 kg/s)

Figure 25 illustrates the static pressure recovery coefficient and the total pressure loss coefficient of the diffuser, plotted against the mass flow rate for different wrap angles. As can be seen in Fig. 25*b*, the minimum destruction of total pressure has occurred at 16.69 kg/s, for all wrap angles. At all flow rates, WA = 25.3º has the lowest $C_{p,s}$ and greatest $C_{p,t}$. The best $C_{p,s}$ can be attributed to WA = 22.3º at all flow rates, however, at the flow rates larger than the design point, the total pressure loss is minimum for WA = 19.3º.

Drawing from the outcomes of this research, it is deducible that WA = 22.3º has the best aerodynamic performance, except close to the choke region, where lower wrap angles show enhanced choke flow rate.

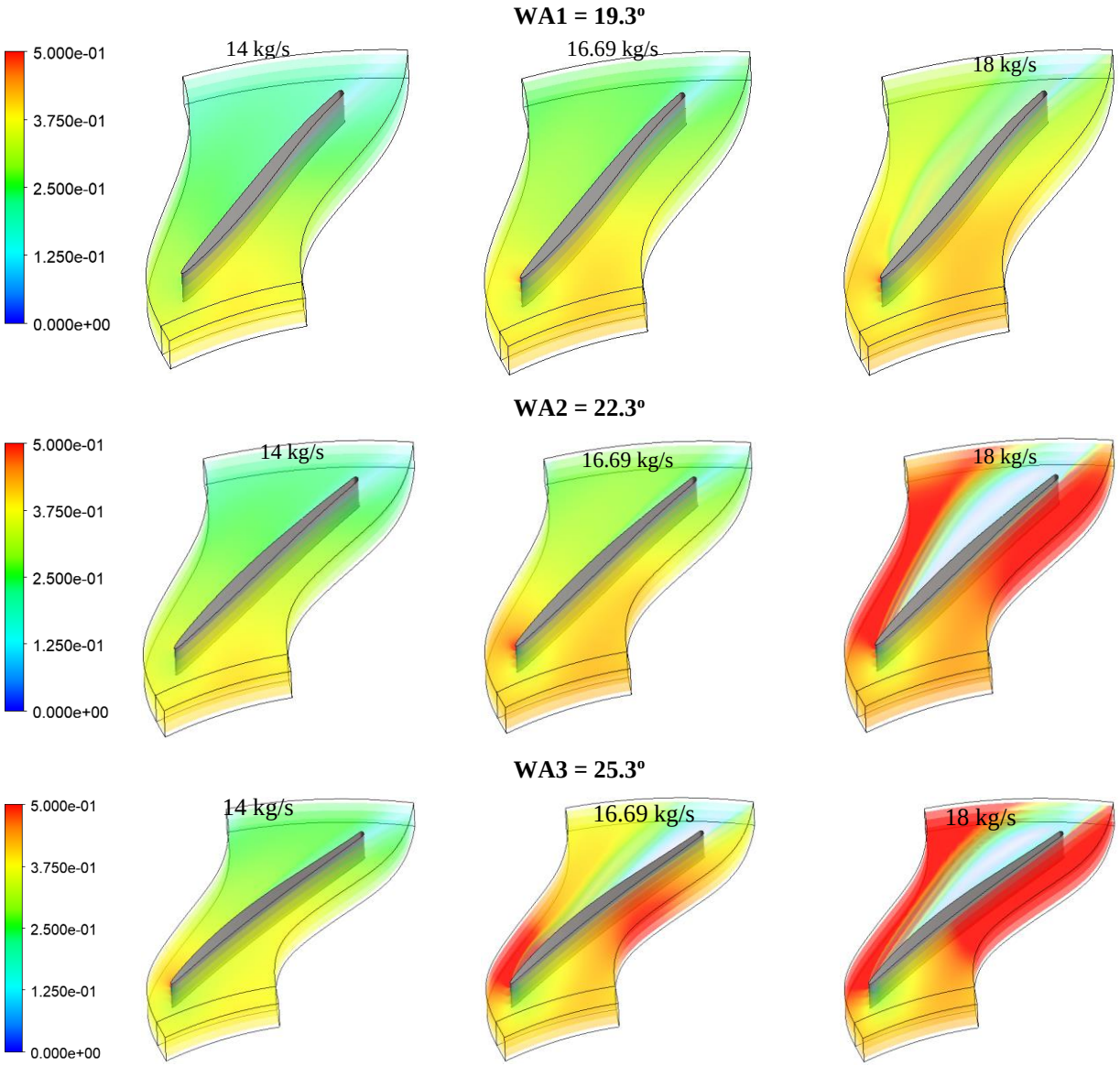

Fig. 24 Volume renderings of the Mach number distributions around the diffuser vanes at various flow rates and wrap angles

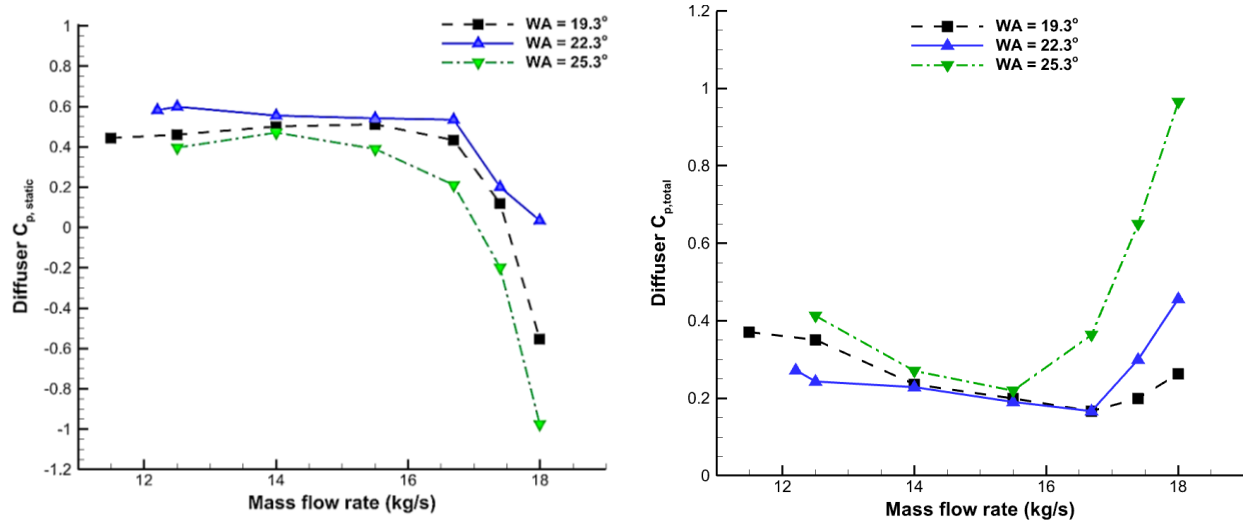

(*a*) (*b*)

Fig. 25 (*a*) Coefficient of static pressure recovery of the diffuser and (*b*) the coefficient of total pressure loss, both plotted against the mass flow rate for a range of wrap angles

5. CONCLUSION

The effects of the diffuser vanes' wrap angle and vane count on the performance of a low pressure-ratio industrial Methane centrifugal compressor are studied using RANS numerical simulations. Three wrap angles (WA=19.3º, 22.3º and 25.3º) and three number of vanes ($N_{Diff.}$=16, 20 and 24) are examined, keeping all the other geometrical and operational parameters constant. The principal conclusions of the present study can be encapsulated in the following points:

- The numerical outcomes derived from the Realizable k-ε turbulence model demonstrated a closer alignment with the experimental results than those obtained using the SST k-ω and RSM turbulence models.
- Reducing the number of diffuser vanes enlarges the operating range of the compressor, however, the pressure ratio will be lower at the flow rates less than the design point. Conversely, higher pressure ratio will be achieved at the flow rates greater than the design flow rate.
- The optimal aerodynamic efficiency of the diffuser, considering both the pressure ratio and the overall efficiency, was achieved when the number of diffuser vanes, N_{Diff}, was set to 20.
- The LE angle of the diffuser vane was adjusted close to the incident flow angle close to the surge flow rate. Therefore, flow separation over the diffuser vanes was observed at higher flow rates, close to the choke flow rate.
- Increasing the diffuser wrap angle, intensifies the flow separation over the diffuser vanes.
- On average, the best performance of the compressor's aerodynamic was occurred at WA = 22.3º.
- Decreasing the wrap angle can enhance the choke flow rate of the compressor, with slight reduction in pressure ratio at lower flow rates.

CONFLICT OF INTEREST

The authors have no conflict of interest to disclose.

AUTHORS CONTRIBUTION

Morteza Anbarsooz: Conceptualization, Data-curation, Formal analysis, Investigation, Methodology, Resources, Software, Validation, Visualization, Writing – original draft, Writing – review & editing, Supervision, Project administration. **Maryam Amiri:** Data-curation, Formal analysis, Investigation, Methodology, Resources, Software, Validation, Visualization. **Ernesto Benini:** Methodology, Resources, Supervision.

REFERENCES

Amiri, M., & Anbarsooz, M. (2019). Improving the energy conversion efficiency of a savonius rotor using automatic valves. *Journal of Solar Energy Engineering, Transactions of the ASME*, *141*(3), 31010–31017. https://doi.org/10.1115/1.4042828

Anbarsooz, M. (2016). Aerodynamic performance of helical Savonius wind rotors with 30° and 45° twist angles: Experimental and numerical studies. *Proceedings of the Institution of Mechanical Engineers, Part A: Journal of Power and Energy*, *230*(6), 523–534. https://doi.org/10.1177/0957650916648828

Anbarsooz, M. (2020). A numerical study on wind dams: A novel approach to enhance wind potential using natural barriers. *Energy Conversion and Management*, *205*, 112454. https://doi.org/https://doi.org/10.1016/j.enconman.2019.112454

Anbarsooz, M., Amiri, M., Erfanian, A., & Benini, E. (2022). Effects of the ring clearance on the aerodynamic performance of a CO2 centrifugal compressors annular seal: A numerical study. *Tribology International*, *170*, 107501. https://doi.org/https://doi.org/10.1016/j.triboint.2022.107501

Anbarsooz, M., Mazloum, M., & Moghadam, D. G. (2020). Converging–diverging ducts for efficient utilization of low-grade wind energy: Numerical and experimental studies. *Journal of Renewable and Sustainable Energy*, *12*(2), 023304. https://doi.org/10.1063/1.5142843

Anish, S., & Sitaram, N. (2009). Computational investigation of impeller-diffuser interaction in a centrifugal compressor with different types of diffusers. *Proceedings of the Institution of Mechanical Engineers, Part A: Journal of Power and Energy*, *223*(2), 167–178. https://doi.org/10.1243/09576509JPE662

Anish, S., Sitaram, N., & Kim, H. D. (2013). A numerical study of the unsteady interaction effects on diffuser performance in a centrifugal compressor. *Journal of Turbomachinery*, *136*(1). https://doi.org/10.1115/1.4023471

ANSYS, Inc. ANSYS manual, Release 19.0. (n.d.).

Ashrafi, F., & Vo, H. D. (2024). Passive flow control at impeller radial bend for stall delay in centrifugal compressors with fishtail pipe diffusers. *Aerospace Science and Technology*, *145*, 108840. https://doi.org/10.1016/j.ast.2023.108840

Baghdadi, S. (1977). The effect of rotor blade wakes on centrifugal compressor diffuser performance-a comparative experiment. *Journal of Fluids Engineering, Transactions of the ASME*, *99*(1), 45–50. https://doi.org/10.1115/1.3448548

Baghdadi, S., & McDonald, A. T. (1975). Performance of three vaned radial diffusers with swirling transonic flow. *Journal of Fluids Engineering, Transactions of the ASME*, *97*(2), 155–160. https://doi.org/10.1115/1.3447238

Benini, E. (2003). Optimal navier-stokes design of compressor impellers using evolutionary computation. *International Journal of Computational Fluid Dynamics*, *17*(5), 357–369. https://doi.org/10.1080/1061856031000099821

Benini, E., & Tourlidakis, A. (2001). *Design optimization of vaned diffusers for centrifugal compressors using genetic algorithms.* 15th AIAA Computational Fluid Dynamics Conference. https://doi.org/10.2514/6.2001-2583

Boncinelli, P., Ermini, M., Bartolacci, S., & Arnone, A. (2007). Impeller-diffuser interaction in centrifugal compressors: Numerical analysis of radiver test case. *Journal of Propulsion and Power*, *23*(6), 1304–1312. https://doi.org/10.2514/1.27028

Casey, M., & Rusch, D. (2014). The matching of a vaned diffuser with a radial compressor impeller and its effect on the stage performance. *Journal of Turbomachinery*, *136*(12). https://doi.org/10.1115/1.4028218

Cellai, A., De Lucia, M., Ferrara, G., Ferrari, L., Mengoni, C. P., & Baldassarre, L. (2003). Application of low solidity vaned diffusers to prevent rotating stall in centrifugal compressors: Experimental investigation. *American Society of Mechanical Engineers, International Gas Turbine Institute, Turbo Expo (Publication) IGTI*, *6 B*, 703–710. https://doi.org/10.1115/GT2003-38386

Clements, W. W., & Artt, D. W. (1989, June 4). *The Influence of Diffuser Vane Leading Edge Geometry on the Performance of a Centrifugal Compressor*. ASME 1989 International Gas Turbine and Aeroengine Congress and Exposition. https://doi.org/10.1115/89-GT-163

Cornelius, C., Biesinger, T., Galpin, P., & Braune, A. (2014). Experimental and computational analysis of a multistage axial compressor including stall prediction by steady and transient CFD methods. *Journal of Turbomachinery*, *136*(6). https://doi.org/10.1115/1.4025583

Dawes, W. N. (1995). A simulation of the unsteady interaction of a centrifugal impeller with its vaned diffuser: flow analysis. *Journal of Turbomachinery*, *117*(2), 213–222. https://doi.org/10.1115/1.2835649

Dawes, W. N. (1992). The simulation of three-dimensional viscous flow in turbomachinery geometries using a solution-adaptive unstructured mesh methodology. *Journal of Turbomachinery*, *114*(3), 528–537. https://doi.org/10.1115/1.2929176

Dean, R. C., & Senoo, Y. (1960). Rotating wakes in vaneless diffusers. *Journal of Fluids Engineering, Transactions of the ASME*, *82*(3), 563–570. https://doi.org/10.1115/1.3662659

Deniz, S., Greitzer, E. M., & Cumpsty, N. A. (1998). *Effects of inlet flow field conditions on the performance of centrifugal compressor diffusers Part 2: Straight-channel diffuser*. Proceedings of the ASME Turbo Expo, 1. https://doi.org/10.1115/98-GT-474

Eckardt, D. (1975). Instantaneous measurements in the jet-wake discharge flow of a centrifugal compressor impeller. *Journal of Engineering for Gas Turbines and Power*, *97*(3), 337–345. https://doi.org/10.1115/1.3445999

El-Askary, W. A., & Nasr, M. (2009). Performance of a bend-diffuser system: Experimental and numerical studies. *Computers and Fluids*, *38*(1), 160–170. https://doi.org/10.1016/j.compfluid.2008.01.003

Engeda, A. (2001a). The design and performance results of simple flat plate flow solidity vaned diffusers. *Proceedings of the Institution of Mechanical Engineers, Part A: Journal of Power and Energy*, *215*(1), 109–118. https://doi.org/10.1243/0957650011536471

Engeda, A. (2001b). The unsteady performance of a centrifugal compressor with different diffusers. *Proceedings of the Institution of Mechanical Engineers, Part A: Journal of Power and Energy*, *215*(5), 585–599. https://doi.org/10.1243/0957650011538820

Engeda, A. (2003). Experimental and numerical investigation of the performance of a 240 kW centrifugal compressor with different diffusers. *Experimental Thermal and Fluid Science*, *28*(1), 55–72. https://doi.org/10.1016/S0894-1777(03)00104-3

Everitt, J. N., & Spakovszky, Z. S. (2012). An Investigation of Stall Inception in Centrifugal Compressor Vaned Diffuser. *Journal of Turbomachinery*, *135*(1). https://doi.org/10.1115/1.4006533

Everitt, J. N., Spakovszky, Z. S., Rusch, D., & Schiffmann, J. (2017). The role of impeller outflow conditions on the performance of vaned diffusers. *Journal of Turbomachinery*, *139*(4). https://doi.org/10.1115/1.4035048

Filipenco, V. G., Deniz, S., Johnston, J. M., Greitzer, E. M., & Cumpsty, N. A. (2000). Effects of inlet flow field conditions on the performance of centrifugal compressor diffusers: Part 1-discrete-passage diffuser. *Journal of Turbomachinery*, *122*(1), 1–10. https://doi.org/10.1115/1.555418

Fujisawa, N., Inui, T., & Ohta, Y. (2019). Evolution process of diffuser stall in a centrifugal compressor with vaned diffuser. *Journal of Turbomachinery*, *141*(4). https://doi.org/10.1115/1.4042249

Galloway, L., Rusch, D., Spence, S., Vogel, K., Hunziker, R., & Kim, S. I. (2018a). An investigation of centrifugal compressor stability enhancement using a novel vaned diffuser recirculation technique. *Journal of Turbomachinery*, *140*(12). https://doi.org/10.1115/1.4041601

Galloway, L., Spence, S., Kim, S. I., Rusch, D., Vogel, K., & Hunziker, R. (2018b). An investigation of the stability enhancement of a centrifugal compressor stage using a porous throat diffuser. *Journal of*

Turbomachinery, *140*(1). https://doi.org/10.1115/1.4038181

Gibson, L., Galloway, L., Kim, S., & Spence, S. (2017). Assessment of turbulence model predictions for a centrifugal compressor simulation. *Journal of the Global Power and Propulsion Society*, *1*, 2II890. https://doi.org/10.22261/2ii890

Goldberg, U., Peroomian, O., & Chakravarthy, S. (1998). A wall-distance-free K-ϵ model with enhanced near-wall treatment. *Journal of Fluids Engineering, Transactions of the ASME*, *120*(3), 457–462. https://doi.org/10.1115/1.2820684

Hah, C., & Krain, H. (1990). Secondary flows and vortex iotion in a high-efficiency backswept impeller at design and off-design conditions. *Journal of Turbomachinery*, *112*(1), 7–13. https://doi.org/10.1115/1.2927425

Halawa, T., Alqaradawi, M., Gadala, M. S., Shahin, I., & Badr, O. (2015). Numerical investigation of rotating stall in centrifugal compressor with vaned and vaneless diffuser. *Journal of Thermal Science*, *24*(4), 323-333. https://doi.org/10.1007/s11630-015-0791-1

Han, G., Yang, C., Wu, S., Zhao, S., & Lu, X. (2023). The investigation of mechanisms on pipe diffuser leading edge vortex generation and development in centrifugal compressor. *Applied Thermal Engineering*, *219*(PB), 119606. https://doi.org/10.1016/j.applthermaleng.2022.119606

Hohlweg, W. C., Direnzi, G. L., & Aungier, R. H. (1993). Comparison of conventional and low solidity vaned diffusers. *American Society of Mechanical Engineers (Paper)*. https://doi.org/10.1115/93-gt-098

Holmes, D., & Connell, S. (1989). *Solution of the 2D Navier-Stokes equations on unstructured adaptive grids.* 9th Computational Fluid Dynamics Conference. American Institute of Aeronautics and Astronautics. https://doi.org/doi:10.2514/6.1989-1932

Hu, C., Yang, X., Zhu, X., & Du, Z. (2018). Stability and structural sensitivity analysis of the turbulent flow in the narrow vaneless diffuser with mean flow method. *Computers and Fluids*, *177*, 46–57. https://doi.org/10.1016/j.compfluid.2018.09.021

Inoue, M., & Cumpsty, N. A. (1984). Experimental study of centrifugal impeller discharge flow in vaneless and vaned diffusers. *Journal of Engineering for Gas Turbines and Power*, *106*(2), 455–467. https://doi.org/10.1115/1.3239588

Issac, J. M., Sitaram, N., & Govardhan, M. (2003). Performance and wall static pressure measurements on centrifugal compressor diffusers. *Proceedings of the Institution of Mechanical Engineers, Part A: Journal of Power and Energy*, *217*(5), 547–558. https://doi.org/10.1243/095765003322407593

Issac, J. M., Sitaram, N., & Govardhan, M. (2004). Effect of diffuser vane height and position on the performance of a centrifugal compressor. *Proceedings of the Institution of Mechanical Engineers, Part A: Journal of Power and Energy*, *218*(8), 647–654. https://doi.org/10.1243/0957650042584320

Jiao, K., Sun, H., Li, X., Wu, H., Krivitzky, E., Schram, T., & Larosiliere, L. M. (2009). Numerical simulation of air flow through turbocharger compressors with dual volute design. *Applied Energy*, *86*(11), 2494–2506. https://doi.org/10.1016/j.apenergy.2009.02.019

Johnston, J. F., & Dean, R. C. (1966). Losses an vaneless diffusers of centrifugal compressors and pumps: Analysis, experiment, and design. *Journal of Engineering for Gas Turbines and Power*, *88*(1), 49–60. https://doi.org/10.1115/1.3678477

Kenny, D. P. (1969). A novel low-cost diffuser for high-performance centrifugal compressors. *Journal of Engineering for Gas Turbines and Power*, *91*(1), 37–46. https://doi.org/10.1115/1.3574671

Kianifar, A., & Anbarsooz, M. (2011). Blade curve influences on the performance of Savonius rotors: Experimental and numerical. *Proceedings of the Institution of Mechanical Engineers, Part A: Journal of Power and Energy*, *225*(3), 343–350. https://doi.org/10.1177/2041296710394413

Kim, Y., Engeda, A., Aungier, R., & Amineni, N. (2002). A centrifugal compressor stage with wide flow range vaned diffusers and different inlet configurations. *Proceedings of the Institution of Mechanical Engineers, Part A: Journal of Power and Energy*, *216*(4), 307–320. https://doi.org/10.1243/09576500260251156

Kirtley, K. (1991). *An algebraic RNG-based turbulence model for three-dimensional turbomachinery flows.* 29th Aerospace Sciences Meeting. American Institute of Aeronautics and Astronautics. https://doi.org/10.2514/6.1991-172

Kirtley, K. R., & Beach, T. A. (1992). Deterministic blade row interactions in a centrifugal compressor stage. *Journal of Turbomachinery*, *114*(2), 304–311. https://doi.org/10.1115/1.2929144

Koumoutsos, A., Tourlidakis, A., & Elder, R. L. (2000). Computational studies of unsteady flows in a centrifugal compressor stage. *Proceedings of the Institution of Mechanical Engineers, Part A: Journal of Power and Energy*, *214*(6), 611–633. https://doi.org/10.1243/0957650001538146

Krain, H. (1981). A study on centrifugal impeller and diffuser flow. *Journal of Engineering for Gas Turbines and Power*, *103*(4), 688–697. https://doi.org/10.1115/1.3230791

Li, Z., Lu, X., Zhang, Y., Han, G., Yang, C., & Zhao, S. (2018). Numerical investigation of a highly loaded centrifugal compressor stage with a tandem bladed impeller. *Proceedings of the Institution of Mechanical Engineers, Part A: Journal of Power and Energy*, *232*(3), 240–253. https://doi.org/10.1177/0957650917725406

Niveditha, P., & Gopi, B. S. (2023). Effect of different types of external guide vanes on the performance of high-pressure centrifugal compressor. *Journal of Applied Fluid Mechanics*, *16*(12), 2556–2568. https://doi.org/10.47176/jafm.16.12.1814

Pullan, G., Young, A. M., Day, I. J., Greitzer, E. M., & Spakovszky, Z. S. (2015). Origins and structure of spike-type rotating stall. *Journal of Turbomachinery*, *137*(5). https://doi.org/10.1115/1.4028494

Rausch, R., Yang, H., & Batina, J. (1991). *Spatial adaption procedures on unstructured meshes for accurate unsteady aerodynamic flow computation.* 32nd Structures, Structural Dynamics, and Materials Conference. American Institute of Aeronautics and Astronautics. https://doi.org/doi:10.2514/6.1991-1106

Reddy, T. C. S., Murty, G. V. R., Mukkavilli, P., & Reddy, D. N. (2004). Effect of the setting angle of a low-solidity vaned diffuser on the performance of a centrifugal compressor stage. *Proceedings of the Institution of Mechanical Engineers, Part A: Journal of Power and Energy*, *218*(8), 637–646. https://doi.org/10.1243/0957650042584294

Rhie, C. M. (1985). A three-dimensional passage flow analysis method aimed at centrifugal impellers. *Computers and Fluids*, *13*(4), 443–460. https://doi.org/10.1016/0045-7930(85)90013-1

Robinson, C., Casey, M., Hutchinson, B., & Steed, R. (2012). *Impeller-diffuser interaction in centrifugal compressors.* Proceedings of the ASME Turbo Expo. https://doi.org/10.1115/GT2012-69151

Senoo, Y., & Ishida, M. (1975). Behavior of severely asymmetric flow in a vaneless diffuser. *Journal of Engineering for Gas Turbines and Power*, *97*(3), 375–383. https://doi.org/10.1115/1.3446012

Senoo, Y., Kinoshita, Y., & Ishida, M. (1977). Asymmetric flow in vaneless diffusers of centrifugal blowers. *Journal of Fluids Engineering, Transactions of the ASME*, *99*(1), 104–111. https://doi.org/10.1115/1.3448501

Shum, Y. K. P., Tan, C. S., & Cumpsty, N. A. (2000). Impeller-diffuser interaction in a centrifugal compressor. *Journal of Turbomachinery*, *122*(4), 777–786. https://doi.org/10.1115/1.1308570

Siva Reddy, T. C., Mukkavilli, P., Ramana Murty, G. V., & Reddy, D. N. (2005). *Some studies on low solidity vaned diffusers of a centrifugal compressor stage.* Proceedings of the ASME Turbo Expo: Vol. 6 PART B (pp. 917–925). https://doi.org/10.1115/GT2005-68972

Siva Reddy, T. C., Ramana Murty, G. V., Prasad, M. V. S. S. S. M., & Reddy, D. N. (2007). Experimental studies on the effect of impeller width on centrifugal compressor stage performance with low solidity vaned diffusers. *Proceedings of the Institution of Mechanical Engineers, Part A: Journal of Power and Energy*, *221*(4), 519–533. https://doi.org/10.1243/09576509JPE373

Skoch, G. J. (2003). Experimental investigation of centrifugal compressor stabilization techniques. *Journal of Turbomachinery*, *125*(4), 704–713. https://doi.org/10.1115/1.1624846

Skoch, G. J. (2005). Experimental investigation of diffuser hub injection to improve centrifugal compressor stability. *Journal of Turbomachinery*, *127*(1), 107–117. https://doi.org/10.1115/1.1812779

Smirnov, P. E., Hansen, T., & Menter, F. R. (2007). *Numerical simulation of turbulent flows in centrifugal compressor stages with different radial gaps.* Proceedings of the ASME Turbo Expo, 6 PART B, 1029–1038. https://doi.org/10.1115/GT2007-27376

Stewart, M. (2019). Dynamic compressors. In M. B. T. S. P. O. Stewart (Ed.), *Surface Production Operations* (pp. 527–653). Gulf Professional Publishing. https://doi.org/10.1016/b978-0-12-809895-0.00008-9

Sun, Z., Zheng, X., & Kawakubo, T. (2018). Experimental investigation of instability inducement and mechanism of centrifugal compressors with vaned diffuser. *Applied Thermal Engineering*, *133*, 464–471. https://doi.org/https://doi.org/10.1016/j.applthermaleng.2018.01.071

Tamaki, H. (2017). Experimental study on the effect of diffuser vane setting angle on centrifugal compressor performance. *Journal of Turbomachinery*, *139*(6). https://doi.org/10.1115/1.4035212

Teipel, I., & Wiedermann, A. (1991). A three-dimensional Euler code for calculating flow fields in centrifugal compressor diffusers. *Computers and Fluids*, *19*(1), 21–31. https://doi.org/10.1016/0045-7930(91)90004-2

Ubben, S., & Niehuis, R. (2014). Experimental investigation of the diffuser vane clearance effect in a centrifugal compressor stage with adjustable diffuser geometry: Part II-detailed flow analysis. *Journal of Turbomachinery*, *137*(3). https://doi.org/10.1115/1.4028298

Ubben, S., & Niehuis, R. (2015). Experimental investigation of the diffuser vane clearance effect in a centrifugal compressor stage with adjustable diffuser geometry-Part I: Compressor performance analysis. *Journal of Turbomachinery*, *137*(3). https://doi.org/10.1115/1.4028297

Vagnoli, S., & Verstraete, T. (2015). URANS analysis of the effect of realistic inlet distortions on the stall inception of a centrifugal compressor. *Computers and Fluids*, *116*, 192–204. https://doi.org/10.1016/j.compfluid.2015.03.015

Wang, P., Qi, M., Mousa, A. M., Ma, C., Yang, C., & Zhu, F. (2022). Numerical and experimental study on temperature and heat transfer characteristics in centrifugal compressor diffuser. *SSRN Electronic Journal*, *228*(March), 120496. https://doi.org/10.2139/ssrn.4251111

Zhu, X., Li, G., Jiang, W., & Fu, L. (2016). Experimental and numerical investigation on application of half vane diffusers for centrifugal pump. *International Communications in Heat and Mass Transfer*, *79*, 114–127. https://doi.org/10.1016/j.icheatmasstransfer.2016.10.015

Ziegler, K. U., Gallus, H. E., & Niehuis, R. (2003a). A study on impeller-diffuser interaction - Part I: Influence on the performance. *Journal of Turbomachinery*, *125*(1), 173–182. https://doi.org/10.1115/1.1516814

Ziegler, K. U., Gallus, H. E., & Niehuis, R. (2003b). A study on impeller-diffuser interaction - Part II: Detailed flow analysis. *Journal of Turbomachinery*, *125*(1), 183–192. https://doi.org/10.1115/1.1516815